# ELECTRON TEMPERATURES IN PLANETARY NEBULAE

JAMES B. KALER
Astronomy Department, University of Illinois

## ABSTRACT

Electron temperatures for 107 planetary nebulae are calculated with the most recent atomic parameters from [O III] or [N II] line intensities or both taken from a variety of sources. The two temperatures exhibit quite different variations with respect to nebular ionization level, or excitation. Within somewhat broad limits, $T_e$[O III] can be taken as constant at 10,200 K for nebulae without He II $\lambda4686$; with the onset of that line, this temperature quickly climbs according to $T_e$[O III] = 9700 K + $58I(\lambda4686)$, where the line intensity is scaled as usual to $I(H\beta) = 100$. $T_e$[N II] behaves oppositely. With $\lambda4686$ present, there is little discernable trend with excitation around a median value of 10,300 K; as the excitation drops and $\lambda4686$ disappears, this temperature appears first to increase, and then to decrease to values well below 8000 K: for log $T_*$ (central star temperature) $<4.7$, $T_e$[N II] = 14,670 log $T_*$ − 57,330. The dispersion in $T_e$ for a specific excitation correlates negatively with O/H as expected.

Combination of the [O III] and [N II] data sets shows that the mean ratio of $T_e$[N II]/$T_e$[O III] = $\bar{r}$ varies smoothly and strongly also as a function of overall nebular excitation. As excitation increases from $T_* \approx$ 25,000 K to ~50,000 K, $\bar{r}$ increases from ~0.7 to ~1.1. It then decreases through the onset of He$^{+2}$, dropping to 0.7 again for the highest levels of ionization, that is, the nebular temperature gradient as inferred from O$^{+2}$ and N$^+$ is usually negative with respect to distance from the central star but reverses to positive for nebulae in the midrange of excitation for $T_* \approx$ 50,000 K.

Comparison of [O III] temperatures among major reference sources shows clear systematic differences. The observations by French and by Torres-Peimbert and Peimbert yield the highest values, roughly 1000 K higher than those obtained from Aller and Czyzak and from Barker. No such trends are seen for $T_e$[N II], possibly because the scatter in the data is considerably larger.

*Subject heading:* nebulae: planetary

## I. BACKGROUND

The strengths of many of the emission lines that are produced in gaseous nebulae, and from which abundances are derived, are very sensitive to electron temperature, which must then be known before the chemical compositions can be found. In addition, temperatures and temperature gradients also provide clues to energy balance and so are important to the construction of theoretical nebular models. Electron temperatures of planetary nebulae have traditionally been derived from the [O III] and [N II] lines. Other forbidden spectra, such as [Ar III], [Ne III], [Ar V], [O I], etc., are available, but they are neither as extensively observed nor have they had their atomic parameters (transition probabilities and target areas) explored so thoroughly. In an abundance analysis, $T_e$[N II] is generally taken to be appropriate to all lower ionization species, and $T_e$[O III] to the higher. Unfortunately, for a large number of objects, values are not available, and one temperature must be inferred from the other, or both must be estimated from some nebular characteristic. The problem is especially severe for higher excitation (ionization level) objects in which the [N II] lines may be inherently weak and the auroral transition at 5754 Å quite unobservable. At the highest excitation, even [O III] $\lambda4363$ may be too weak for detection, and $T_e$ must be guessed. At the low-excitation extreme, $T_e$[O III] may have to be assumed from $T_e$[N II].

In their extensive study of planetaries, Torres-Peimbert and Peimbert (1977) found that for lower levels of ionization $T_e$[N II] = $T_e$[O III], whereas for those with $I$(He II $\lambda4686$) > 25 [on the usual scale $I(H\beta) = 100$], $T_e$[N II] =

$T_e$[O III]/1.25. Kaler (1978a) preferred equality for $I(\lambda4686)$ up to 60, thence $T_e$[N II] = $T_e$[O III]/1.4; the divisor was later returned to 1.2 by Kaler (1983).

From the above work there is little doubt that the [N II] temperature is below the [O III] value for higher excitation objects. But the detailed relationship between the two has not been explored, largely because of the lack of a sufficiently large body of data. The problem is approached in this study by merging all the available large data sets with several additional observations to generate temperatures for 107 nebulae, sufficient to illustrate the trends in the values over most of the range of nebular excitation.

## II. DERIVATION OF TEMPERATURE

For several decades we have employed standard formulae for the calculation of electron temperatures, which can be derived from simplifications of the $p^2$ equilibrium solutions (see, e.g., Seaton 1960; Osterbrock 1974; Kaler et al. 1976; Aller 1984). The coefficients of these equations have slowly evolved as the atomic parameters have been improved. The most recent compilation by Mendoza (1983) yields the following formulae:

$$T_e[\text{O III}] = \frac{14320}{\log R_O - 0.890 + \log (1 + 0.046x)} \quad (1)$$

and

$$T_e[\text{N II}] = \frac{10860}{\log R_N - 0.841 + \log (1 + 0.251x)}, \quad (2)$$

322

# TABLE 1
## [O III] AND [N II] ELECTRON TEMPERATURES: THE COMPLETE DATA SET

| Nebula (1) | Ref (2) | $T_e$ (K) [O III] (3) | $T_e$ (K) [N II] (4) | $x_0{}^{a}$ (5) | $x_N{}^{a}$ (6) |
|---|---|---|---|---|---|
| NGC 40 | AC1 | ... | 8040 | 0.20 | 0.12 |
| | CSPT | 10980 | 7660 | 0.29 | 0.27 |
| NGC 650 | AC2 | 10660 | 9520 | 0.01 | |
| NGC 1535 | AC2 | 11210 | ... | 0.30 | |
| | GMC | 11970 | ... | 0.25 | |
| | PTP | 11380 | ... | 0.30 | |
| | TPP | 12120 | ... | 0.19 | |
| NGC 2022 | AC2 | 14380 | ... | 0.10 | |
| | TPP | 15400 | ... | 0.22 | 0.03 |
| NGC 2346 | AC1 | 13640 | ... | (0.10) | |
| NGC 2371 | AC2-E | 12520 | 9690 | 0.22 | 0.10 |
| | AC2-W | 11100 | 9290 | 0.22 | 0.10 |
| | O | 16810 | ... | 0.22 | |
| | TPP-a | 14630 | 9900 | 0.22 | 0.14 |
| | TPP-b | 15580 | ... | 0.22 | 0.14 |
| NGC 2392 | AC1 | 13750 | 10140 | 0.0 | 0.33 |
| | BAR | 15050 | 12690 | 0.05 | |
| | O | 17730 | ... | 0.33 | |
| | TPP | 16520 | ... | 0.33 | |
| NGC 2438 | TPP | 10870 | ... | 0.05 | |
| NGC 2440 | GMC | 13930 | 10260 | 0.50 | 0.25 |
| | SAKC | 13640 | 9790 | 0.50 | 0.33 |
| | TPP | 14330 | 10120 | 0.50 | 0.22 |
| NGC 2452 | AC1-a | 11040 | 9490 | 0.14 | 0.24 |
| | AC1-b | 12220 | 8900 | 0.45 | 0.35 |
| | AC1-c | 10440 | 8780 | 0.10 | 0.20 |
| | TPP | 12950 | ... | 0.22 | |
| NGC 2610 | TPP-a | 18230 | ... | (0.10) | |
| | TPP-b | 17170 | ... | | |
| NGC 2792 | TPP | 14820 | | (0.10) | |
| NGC 2818 | DU | 14800 | 11380 | (0.10) | |
| | TPP | 15520 | 12510 | | |
| NGC 2867 | AKRM | 11240 | 9180 | 0.89 | 0.20 |
| | GMC | 11930 | 10330 | | |
| NGC 3132 | TPP-b | 9760 | 8920 | 0.06 | |
| | TPP-c | 9630 | 9440 | | |
| | TPP-d | 10640 | 9060 | | |
| | TPP-e | ... | 8170 | | |
| NGC 3211 | TPP | 14320 | ... | (0.10) | |
| NGC 3242 | AC1 | 11370 | 10060 | 0.30 | |
| | BAR | 11370 | ... | 0.50 | |
| | B85-1 | 11460 | ... | | |
| | B85-2 | 11060 | ... | | |
| | B85-3 | 11170 | ... | | |
| | B85-4 | 11160 | ... | | |
| | B85-5 | 10620 | ... | | |
| | TPP | 12300 | ... | | |
| NGC 3587 | TPP-a | 10910 | ... | (0.10) | |
| NGC 3918 | TPP | 12490 | 9280 | 0.56 | |
| NGC 4361 | BAR | 19370 | ... | (0.01) | |
| | TPP-a | 18950 | ... | | |
| | TPP-b | 21000 | ... | | |
| | TPP-c | 19470 | ... | | |
| NGC 5307 | TPP | 12680 | ... | 0.6 | |
| NGC 5315 | TPP | 9210 | 10200 | 3.0 | |
| NGC 5873 | GMC | 13070 | ... | 0.8 | |
| NGC 5882 | GMC | 9280 | 8290 | 1.1 | |
| | TPP | 9410 | 8940 | | |
| NGC 6058 | K | 13200 | ... | 0.20 | |
| NGC 6210 | AC2 | 9710 | ... | 0.40 | |
| | BAR | 9570 | 9650 | 0.43 | |
| | FR | 9850 | 11830 | 0.32 | |
| NGC 6302 | AC78 | 15610 | 16380 | 3.5 | 0.78 |
| | DFP | 17380 | ... | 3.8 | |
| NGC 6309 | AC2 | 11250 | 9850 | 0.71 | 0.40 |
| NGC 6537 | FAKC | 15720 | 16760 | 1.26 | 0.63 |
| NGC 6543 | AC1 | 8230 | 9680 | 0.74 | 0.40 |
| | BAR3 | 7890 | 8220 | 0.59 | |
| NGC 6567 | BAR | 10950 | 15180 | 1.2 | |
| NGC 6572 | AC1 | 9770 | ... | 1.3 | 1.2 |
| | BAR3 | ... | 11780 | | |
| | FR | 10170 | 11880 | | |
| | OPC | 11490 | ... | | |
| | PTP-EW | 9930 | ... | | |
| | PTP-LA | 10170 | 12620 | | |
| NGC 6644 | BAR | 12600 | 13620 | 0.50 | |
| NGC 6720[b] | BAR | 10570 | 9730 | 0.08 | |
| | BAR4-1 | 11490 | 13840 | 0.12 | |
| | BAR4-3a | 10260 | 13235 | 0.14 | |
| | BAR4-4 | 9330 | 9220 | 0.15 | |
| | (BAR4-6) | 11200 | 10180 | 0.12 | |
| | FR | 11380 | 9990 | 0.06 | |
| | HM-1 | 16560 | 12720 | 0.10 | |
| | HM-2 | 10580 | 10350 | | |
| | HM-3 | 10500 | 8080 | | |
| | HM-4 | 9630 | 9070 | | |
| | (HM-5) | ... | 10050 | | 0.07 |
| | (HM-6) | ... | 8820 | | 0.04 |
| | PTP | 10900 | 10040 | 0.10 | |
| NGC 6751 | AC1 | 10330 | 7910 | 0.0 | 0.37 |
| NGC 6765 | K | 11700 | 8740 | 0.05 | |
| NGC 6778 | AC2 | 7950 | 7730 | 0.20 | 0.08 |
| NGC 6790 | AC1 | 11780 | 16700 | 0.63 | 1.0 |
| | FR | 13740 | 17340 | | |
| NGC 6803 | PTP | 9630 | 10160 | 1.0 | 0.37 |
| NGC 6804 | K | 12900 | ... | 0.07 | |
| NGC 6818 | AC1 | 12820 | 11410 | 0.25 | 0.22 |
| NGC 6826 | AC2 | 10560 | 12240 | 0.40 | 0.25 |
| | FR | 11390 | ... | | |
| | O | 11530 | ... | | |
| NGC 6833 | BAR | 13160 | 20900 | 0.70 | |
| NGC 6853[c] | B84-1 | 11810 | 8640 | 0.03 | |
| | B84-2 | 11260 | 10130 | | |
| | B84-3 | 10850 | 9620 | | |
| | B84-4 | 9880 | 9560 | | |
| | B84-5 | 9930 | 10150 | | |
| | (B84-6) | 12300 | 9220 | | |
| | (B84-7) | 8930 | 10610 | | |
| | HM4-1 | 11910 | 11140 | | |
| | HM4-2 | 11720 | 10620 | 0.05 | |
| | (HM4-3) | 8690 | 8550 | 0.05 | |
| | (HM4-4) | 12620 | 9210 | 0.03 | |
| | (HM4-5) | 13410 | 9130 | 0.08 | |
| | (HM4-6) | 16700 | 9400 | 0.05 | |
| NGC 6884 | AC1 | 10890 | 13750 | 0.63 | |
| | PTP | 9680 | 9860 | 0.75 | 0.64 |
| NGC 6886 | AC1 | 12970 | 10600 | 1.0 | 0.63 |
| NGC 6894 | K | ... | 9900 | | 0.02 |
| NGC 6905 | AC1 | 12130 | ... | 0.10 | |
| NGC 7009[d] | B83-1 | 10300 | ... | 0.40 | |
| | B83-2 | 9370 | ... | | |
| | B83-3 | 9780 | ... | | |
| | B83-4 | 9190 | 9710 | 0.36 | |
| | B83-5 | 9710 | 11370 | 0.26 | |
| | B83-6 | 9900 | ... | 0.40 | |
| | (B83-7) | 11760 | 11760 | 0.43 | |
| | BAR3-A1 | 10060 | ... | 0.66 | 0.47 |
| | BAR3-A2 | 9870 | ... | | |
| | BAR3-B | 9810 | ... | | |
| | CA-1 | 9840 | 12540 | 0.79 | 0.45 |
| | CA-2 | 9070 | 10430 | 0.50 | |
| | (CA-3) | 9700 | 9340 | 0.17 | |
| | (FR) | 12270 | 13370 | | |
| | OPC | 11200 | ... | 0.66 | |
| | PTP | 9700 | 10980 | 0.66 | 0.47 |
| NGC 7026 | AC1 | 9050 | 9510 | 0.80 | |
| NGC 7027 | BAR | 12220 | 14150 | 13.5 | 4.5 |
| | BAR3-A2 | ... | 13490 | | |

TABLE 1—*Continued*

| Nebula (1) | Ref (2) | $T_e$ (K) [O III] (3) | $T_e$ (K) [N II] (4) | $x_O$ (5) | $x_N$ (6) | Nebula (1) | Ref (2) | $T_e$ (K) [O III] (3) | $T_e$ (K) [N II] (4) | $x_O$ (5) | $x_N$ (6) |
|---|---|---|---|---|---|---|---|---|---|---|---|
| | (FR) | 14240 | 15310 | | | IC 4593 | BAR | 8920 | 11390 | 0.89 | 0.20 |
| | KACE | 12480 | 13220 | | | IC 4634 | AC2 | 9740 | 11150 | 0.52 | 0.79 |
| | MM-1 | 12590 | 14655 | | | IC 4776 | AC2 | 8590 | 13870 | 0.89 | 1.26 |
| | MM-2 | 12130 | 13380 | | | IC 4846 | AC1 | 9940 | 13760 | 1.0 | 0.40 |
| | MM-3 | 13240 | 14630 | | | | BAR | 10020 | 9650 | | |
| | MM-A | 12180 | ... | | | IC 5117 | AC1 | 11620 | 12530 | 7.1 | 4.0 |
| | (O) | 12360 | 15800 | | | IC 5217 | AC1 | 11360 | 11470 | 0.56 | 1.0 |
| | PTP | 12260 | 12020 | | | | BAR | 11340 | 10480 | 0.69 | |
| NGC 7293[e] | H-A1 | 10870 | 8650 | 0.01 | | | FR | 12330 | 14020 | 0.25 | |
| | H-A2 | ... | 8570 | 0.08 | | | PTP | 11240 | ... | 0.50 | |
| | H-A3 | 10890 | 9430 | 0.01 | | BB-1 | HM2 | 12910 | 10800 | 0.14 | |
| | H-A4 | 8630 | 9110 | 0.02 | | | TRP | 12910 | 10120 | | |
| | H-B1 | 10520 | 9180 | 0.01 | | BD+30° | PTP | ... | 8570 | 0.56 | |
| | H-B2 | 12240 | 9110 | 0.06 | | Cn3-1 | AC1 | 22190 | 6450 | 1.0 | |
| | H-B3 | 11360 | 10810 | 0.01 | | | BAR | 21520 | 6660 | | |
| | H-B4 | 12140 | 9880 | 0.18 | | | FR | 20760 | 8520 | | |
| NGC 7662[f] | AC2 | 13560 | 9840 | 0.38 | 0.28 | DDM-1 | BC | 11820 | 11890 | 0.40 | |
| | B86-1 | 13910 | ... | (0.01) | | Ha1-55 | PR | ... | 5300 | | 0.4 |
| | B86-2 | 13260 | ... | (0.01) | | Ha4-1 | HM2 | 11910 | 10280 | 0.03 | |
| | B86-3 | 12420 | ... | 0.08 | | | TPP2 | 12160 | ... | | |
| | B86-4 | 11680 | ... | 0.40 | | He2-5 | GMC | 10960: | 11540 | 0.73 | |
| | B86-5 | 11430 | 11390 | 0.35 | | He2-7 | GMC | 12670 | 12870 | 0.26 | |
| | BAR3-A1 | 13770 | ... | 0.27 | | He2-108 | TPP | 9650 | ... | 0.2 | |
| | BAR3-B | 12780 | ... | | | He2-131 | TPP | ... | 7110 | | 2.0 |
| | FR | (15150) | ... | | | Hu1-1 | AC1 | 12840 | 10150 | .25 | .17 |
| | O | 12730 | ... | | | | BAR | 11430 | 10230 | | .26 |
| | PTP | 12910 | | | | Hu1-2 | AC2 | 17070 | 11590 | .69 | .56 |
| IC 351 | AC2 | 12300 | ... | 0.25 | | Hu2-1 | AC2 | 8870 | 12600 | .35 | .61 |
| | BAR | 11870 | ... | | | | BAR | 8480 | 12160 | | .23 |
| | TPP | 11890 | ... | | | | FR | 11580 | 15000 | | .89 |
| IC 418 | AC2 | 8420 | 8450 | 1.4 | | J 320 | AC2 | 12350 | 11590 | 0.40 | |
| | BAR | 7460 | 8800 | | | | BAR | 12880 | 15650 | 0.10 | |
| | BAR3-A1 | 11160 | ... | | | J 900 | AC2 | 12060 | 10610 | 0.64 | 0.38 |
| | BAR3-A2 | 12600 | ... | | | M1-1 | AC1 | 15480 | ... | 0.30 | |
| | BAR3-A3 | ... | 7380 | | | | BAR | 14510 | 7340 | 0.36 | |
| | BAR3-B | 9960 | ... | | | M1-4 | K | 12800 | ... | 0.13 | |
| | GMC | 9540 | 8730 | 1.8 | 1.12 | M1-5 | BAR | 9090 | 11710 | 0.28 | |
| | (O) | 13300 | 9190 | 1.4 | | M1-14 | TPP | 10530 | 9750 | 0.50 | |
| | PTP | 9500 | 8960 | | | M1-41 | DO4-A | ... | 10860 | 0.14 | |
| | TPP | 9280 | 8450 | | | M1-67 | BAR | ... | 7350 | | 0.14 |
| IC 1297 | GMC | 10820 | 8340 | 1.26 | | M1-74 | AC2 | 9450 | 12100 | 3.2 | 2.1 |
| IC 1747 | BAR | 10130 | ... | 0.33 | | | BAR | 9060 | 9470 | 3.7 | |
| | AC1 | 10150 | ... | 0.22 | | M2-9 | BAR-S | 21280 | 9420 | 0.32 | |
| IC 2003 | AC2 | 11850 | 13180 | 0.45 | 0.66 | | BAR-N | 8720 | 9010 | 0.35 | |
| | BAR | 13160 | 16640 | 0.16 | | M2-50 | BAR | 12220 | ... | 1.5 | |
| | TPP | 11340 | ... | 0.31 | | M3-1 | GMC | 12290 | 9900 | 0.56 | |
| IC 2149 | BAR | 9730 | 8900 | 0.34 | | M3-35 | BAR | 9010 | 11200 | 8 | |
| | O | 10890 | ... | | | M4-18 | GD | ... | 6800 | | 2 |
| | TPP | 10270 | 8480 | | | Me2-1 | AKC | 13100 | 11570 | 0.13 | 0.14 |
| IC 2165 | AC1 | 13850 | 11740 | 0.32 | | | K | 11750 | ... | 0.35 | |
| | GMC | 13610 | 9140 | 0.56 | | Me2-2 | BAR | 10790 | 13240 | 0.56 | |
| | TPP | 14270 | 8320 | | | PB-4 | TPP | 10770 | ... | 1.2 | |
| IC 2448 | TPP | 13120 | ... | (0.10) | | PB-6 | TPP | 14370 | 11920 | 0.2 | |
| IC 2501 | TPP | 9870 | 9940 | 1.0 | | Ps-1 | HM2 | 12250 | ... | 0.3 | |
| IC 2553 | GMC | 10100 | 11690 | 0.79 | | | P72 | 14260 | ... | | |
| IC 2621 | GMC | 13190 | 9860 | 2.0 | | | TPP2 | 12720 | ... | | |
| IC 3568 | BAR | 10410 | ... | 0.31 | | Sn-1 | BAR | 10020 | ... | 0.08 | |
| IC 4191 | GMC | 10470 | 12580 | 1.8 | 0.63 | Vy1-2 | BAR | 9650 | 7700 | 0.25 | |
| IC 4406 | TPP | 10480 | 9370 | (0.10) | | | | | | | |

[a] Values in parentheses are estimates. If there is no entry for $x$ for a given source, it is the same as the entry immediately above.

[b] Individual extinctions used for the BAR4 and HM regions. BAR4–6 and HM-5 and HM-6 excluded from averages, as indicated here and elsewhere by parentheses.

[c] Individual extinctions used for the HM4 regions. B84–6 and B84–7 and HM4–3–HM4–6 excluded from averages.

[d] B83–7 and CA-3 are in the ansae and are excluded from averages, as is FR.

[e] Individual extinctions used for the H-A regions.

[f] Individual extinctions used for the B86 regions. FR is excluded from averages.

REFERENCES (in alphabetical order).—(AC1) Aller and Czyzak 1979. (AC2) Aller and Czyzak 1983. (AC78) Aller and Czyzak 1978. (AKC) Aller *et al.* 1981*a*. (AKRM) Aller *et al.* 1981*b*. (BAR) Barker 1978. (BAR3) Barker 1979. (BAR4) Barker 1980. (B83) Barker 1983. (B84) Barker 1984. (B85) Barker 1985. (B86) Barker 1986. (BC) Barker and Cudworth 1984. (CA) Czyzak and Aller 1979. (CSPT) Clegg *et al.* 1983. (DFP) Danziger *et al.* 1973. (DO4) Dopita 1977. (DU) Dufour 1984. (FAKC) Feibelman *et al.* 1985. (FR) French 1981. (GD) Goodrich and Dahari 1985. (GMC) Gutiérrez-Moreno *et al.* 1985. (H) Hawley 1978. (HM) Hawley and Miller 1977). (HM2) Hawley and Miller 1978*a*. (HM4) Hawley and Miller 1978*b*. (K) Kaler 1985. (KACE) Kaler *et al.* 1976. (MM) Miller and Mathews 1972. (O) O'Dell 1963. (OPC) O'Dell 1964. (P72) Peimbert 1973. (PR) Price 1981. (PTP) Pembiert and Torres-Peimbert 1971. (SAKC) Shields *et al.* 1981. (TPP) Torres-Peimbert and Peimbert 1977. (TPP2) Torres-Peimbert and Peimbert 1979. (TRP) Torres-Peimbert *et al.* 1981.

where $R_O$ and $R_N$ are for [O III] and [N II] respectively the ratios of the intensities of the nebular lines to that of the auroral line, corrected for interstellar extinction, or

$$R_O = \frac{I(\lambda 4959) + I(\lambda 5007)}{I(\lambda 4363)} \; ; \quad R_N = \frac{I(\lambda 6548) + I(\lambda 6584)}{I(\lambda 5754)} \; . \quad (3)$$

In equations (1) and (2), $x$ is an electron density parameter equal to $10^{-2} N_e/\sqrt{T_e}$, where $N_e$ is the electron density of the nebula. The target areas $\Omega$ change slowly as a function of temperature, and strictly speaking we should iterate on the equations' coefficients. However, the change is so small that the error produced at 20,000 K by using 10,000 K target areas is less than 200 K, which is lost in the observational uncertainties, and only the 10,000 K values are adopted above. The second order density corrections given by Aller (1984) are unnecessary for the objects considered here.

All temperatures calculated from all observational studies are presented in Table 1. The nebula name is given in column (1), and a reference code in column (2); a reference key is provided at the end of the table. Multiple observations of a single nebula from a reference source are indicated by the author's code for the region observed following the reference. Columns (3) and (4) give the [O III] and [N II] electron temperatures, and columns (5) and (6) the respective values of $x$ ($x_O$ and $x_N$) used to compute them. These are found from the nebular [O II], [S II], and [Cl III] doublets, also using Mendoza's (1983) compilation. Where the observations are available, the values of $x$ are chosen to be appropriate to the ionization potentials of $O^{+2}$ and $N^+$, so that [Cl III] is used to find $x_O$ and the other two to determine $x_N$. Ionic stratification is present for most objects, and different authors select different nebular regions for examination. Where possible, the density parameters were derived from the same work as were the temperatures. Otherwise, a mean of all available data is used from the compilation by Kaler (1976a) and from Aller and Epps (1976). In instances where a single value of $x$ is used for both temperatures, it is centered between colums (5) and (6).

Before the calculation of the temperatures, all the data were corrected for interstellar reddening, using the Whitford (1958) extinction function expressed in the common form used in nebular spectrophotometry, wherein the true line intensity equals that observed times $10^{cf(\lambda)}$, where $c$ is the logarithmic extinction at H$\beta$. For purposes of correcting the line ratios, $\Delta f[\text{O III}] = f(\lambda 4363) - f(\lambda 4991) = 0.16$ and $\Delta f[\text{N II}] = 0.145$. In order that all nebulae be treated consistently, all extinctions (with exceptions as noted) were derived from mean H$\alpha$ line intensities, for which $f(\text{H}\alpha) = -0.335$, and Brocklehurst's (1971) theoretical ratio of 2.85. The H$\alpha$ data come from the references of Table 1 as well as from others given by Kaler (1976a). Several authors, notably Torres-Peimbert and Peimbert (1977); Aller and Czyzak (1979, 1983); and Gutiérrez-Moreno, Moreno, and Cortés (1985) provide data already corrected for extinction with somewhat different extinction curves and constants. In all cases but one, these were converted to the system used here, with the original observed H$\alpha$ intensity used in the mean from which $c$ was derived. The exception is Aller and Czyzak (1979), who provide insufficient data for such conversion, and whose intensities were used in their published state. In all cases, the Aller and Czyzak (1983) data supersede those from Aller and Czyzak (1979). The resulting extinctions, used for all reference sources for a given object, are in column (8) of Table 2, which gives a variety of other single-valued nebular parameters. Exceptions are those large nebulae that exhibit possible variations in extinction across their surfaces. In these cases, noted in the footnotes to Table 1, the observed extinctions were employed for the specified regions. The other observations of these objects were corrected with the means given in Table 2.

Mean observed electron temperatures are listed in Table 2. These are simply straight averages of those presented in Table 1, excluding the values for which the reference code is set into parentheses. These latter either subjectively differ too much from a well-established mean or are appropriate to the outer shells or to peripheral nebular regions, as observed for NGC 6720, 6853, and 7009 (see the footnotes to Table 1). In Table 1, all temperatures are given to the nearest 10 K, however unrealistic that may be, with the means rounded to the nearest 100 K in Table 2.

Next, let the ratio of the two temperatures for any single entry (any reference or any region of any reference) be $r = T_e[\text{N II}]/T_e[\text{O III}]$. The mean ratio $\bar{r}$ is given in column (4) of Table 2. Note that $\bar{r}$ is the average of individual ratios, not the ratio of the mean temperatures.

Figures 1–6 display comparisons among the major reference sources. The first three show $T_e[\text{O III}]$ for Aller and Czyzak (1979, 1983), Barker (1983), and Torres-Peimbert and Peimbert (1977) plotted against the values derived from the other sources for mutually observed nebulae. The second three are the same for $T_e[\text{N II}]$. Temperatures for different regions observed by a given reference source are averaged. It is immediately evident that significant systematic shifts exist among the various sets of $T_e[\text{O III}]$. Aller and Czyzak average about 1000 K lower than Torres-Peimbert and Peimbert, French (1981), and "other," but agree quite well with Barker. There seems to be no noticeable difference between Aller and Czyzak (1979) and (1983). The shifts could be caused by systematic errors in the line intensities, or they may be real. Various individuals use different aperture sizes and may set systematically on different positions within the nebulae, and thus the differences could represent internal temperature gradients. If the problem is caused by errors, there is no way of determining who, if anyone, might be correct, so that no attempt is made to adjust the final values. The mean [O III] temperatures of Table 2, however, are not then entirely internally consistent, since they arise from different combinations of data that contain different errors or shifts. These systematic trends are not seen among the [N II] temperatures, which exhibit considerably more scatter, probably because of the weakness of the auroral line.

### III. CORRELATIONS

We now proceed to examine the dependence of the [O III] and [N II] electron temperatures on various nebular parameters. In part, the purpose is to establish correlations that will allow us to estimate $T_e$ when the pertinent spectral data are not available. Kaler (1970) clearly showed from the primarily photographic spectra of the time that $T_e$ was empirically related not only to the abundance of oxygen, but also to the level of nebular ionization. With the improved data of Table 2, we may now refine that study and expand it to examine other correlations. The ionization level is characterized here by the strength of He II $\lambda 4686$ for higher excitation objects, and by the central star temperature (specifically log $T_*$) for the lower excitation nebular that do not contain $He^{+2}$. These two are arranged along a continuous sequence wherein log $T_* = 4.75$ corresponds to $I(\lambda 4686) = 0$. This system is essentially an empirical

TABLE 2

MEAN [O III] AND [N II] ELECTRON TEMPERATURES AND SUPPORTING PARAMETERS

| Nebula | $\overline{T}_e$ (K) [O III] | [N II] | $\overline{r}$ | I($\lambda4686$) or log $T_*{}^a$ | $10^4$ O/H | log [O II]/[O III] | c |
|--------|------|--------|----|----------|-----|----------|-----|
| (1) | (2) | (3) | (4) | (5) | (6) | (7) | (8) |
| NGC   40 | 11000 | 7900 | 0.70 | 4.51 | 3.6 | 1.35 | 0.76 |
| NGC  650 | 10700 | 9500 | 0.89 | 56 | 8.0 | −0.41 | 0.33 |
| NGC 1535 | 11700 | ... | ... | 15 | ... | ... | 0.10 |
| NGC 2022 | 14900 | ... | ... | 93 | ... | ... | 0.43 |
| NGC 2346 | 13600 | ... | ... | 22 | 2.1 | ... | 0.89 |
| NGC 2371 | 14100 | 9600 | 0.76 | 94 | ... | −1.28 | 0.13 |
| NGC 2392 | 15800 | 11400 | 0.79 | 45 | 3.2 | −1.19 | 0.17 |
| NGC 2438 | 10900 | ... | ... | 42 | 6.9 | ... | 0.20 |
| NGC 2440 | 14000 | 10100 | 0.72 | 69 | 5.1 | −1.06 | 0.33 |
| NGC 2452 | 11700 | 9100 | 0.81 | 62 | 5.7 | −1.20 | 0.55 |
| NGC 2610 | 17800 | ... | ... | 95 | ... | ... | 0.03 |
| NGC 2792 | 14800 | ... | ... | 93 | ... | ... | 0.79 |
| NGC 2818 | 15200 | 12000 | 0.79 | 76 | ... | −0.67 | 0.30 |
| NGC 2867 | 11600 | 9800 | 0.84 | 30 | ... | −1.19 | 0.40 |
| NGC 3132 | 10000 | 8900 | 0.92 | 16 | 6.7 | −0.12 | 0.16 |
| NGC 3211 | 14300 | ... | ... | 76 | 5.1 | ... | 0.26 |
| NGC 3242 | 11300 | 10100 | 0.88 | 27 | 4.2 | −2.18 | 0.08 |
| NGC 3587 | 10900 | ... | ... | 11 | 3.3 | ... | 0.00 |
| NGC 3918 | 12500 | 9300 | 0.74 | 38 | 6.4 | −1.56 | 0.27 |
| NGC 4361 | 19700 | ... | ... | 115 | ... | ... | 0.00 |
| NGC 5307 | 12700 | ... | ... | 20 | 2.8 | ... | 0.41 |
| NGC 5315 | 9200 | [10200] | 1.11 | 4.75/6 | 4.2 | −1.31 | 0.68 |
| NGC 5873 | 13100 | ... | ... | 46 | ... | ... | 0.14 |
| NGC 5882 | 9300 | [ 8600] | 0.92 | 4.79/4 | 4.6 | −1.96 | 0.39 |
| NGC 6058 | 13200 | ... | ... | 69 | ... | ... | 0.04 |
| NGC 6210 | 9700 | 10700 | 1.10 | 4.76 | 4.6 | −1.55 | 0.03 |
| NGC 6302 | 16500 | 16400 | 1.05 | 63 | 2.8 | ... | 1.13 |
| NGC 6309 | 11300 | 9900 | 0.88 | 73 | ... | −2.04 | 0.78 |
| NGC 6537 | 15700 | 16800 | 1.07 | 80 | ... | −1.78 | 2.04 |
| NGC 6543 | 8100 | 9000 | 1.11 | 4.65 | 5.4 | −1.63 | 0.12 |
| NGC 6567 | 11000 | [15200] | 1.39 | 4.75 | 2.9 | −1.72 | 0.75 |
| NGC 6572 | 10300 | [12100] | 1.20 | 4.78 | 3.2 | −1.52 | 0.34 |
| NGC 6644 | 12600 | 13600 | 1.08 | 18 | 3.5 | −1.56 | 0.38 |
| NGC 6720 | 11100 | 10600 | 0.97 | 28 | 4.1 | −0.76 | 0.29 |
| NGC 6751 | 10300 | 7900 | 0.77 | 36 | 7.1 | −0.78 | 1.08 |
| NGC 6765 | 11700 | 8700 | 0.75 | 71 | ... | −1.02 | 0.60 |
| NGC 6778 | 8000 | 7700 | 0.97 | 10 | ... | −0.78 | 0.89 |
| NGC 6790 | 12800 | (17000) | 1.34 | 4.82/3 | 3.8 | −1.99 | 0.82 |
| NGC 6803 | 9600 | 10200 | 1.06 | 4.79/4 | 4.4 | −1.50 | 0.79 |
| NGC 6804 | 12900 | ... | ... | 97 | ... | ... | 0.91 |
| NGC 6818 | 12800 | 11400 | 0.89 | 53 | 4.5 | −1.55 | 0.31 |
| NGC 6826 | 11200 | 12200 | 1.16 | 4.67 | 3.1 | −1.69 | 0.03 |
| NGC 6833 | 13200 | 20900 | 1.59 | 4.69/2 | 1.2 | −1.80 | 0.19 |
| NGC 6853 | 11000 | 10000 | 0.91 | 33 | 5.1 | −0.60 | 0.17 |
| NGC 6884 | 10300 | 11800 | 1.14 | 10 | 4.7 | −1.71 | 0.76 |
| NGC 6886 | 13000 | 10600 | 0.82 | 42 | 5.2 | −1.06 | 0.76 |
| NGC 6894 | ... | 9900 | ... | 9 | ... | −1.02 | 0.88 |
| NGC 6905 | 12100 | ... | ... | 90 | ... | ... | 0.93 |
| NGC 7009 | 9800 | 11000 | 1.16 | 14 | 3.6 | −1.85 | 0.07 |
| NGC 7026 | 9100 | 9500 | 1.05 | 11 | 5.7 | −1.17 | 0.66 |
| NGC 7027 | 12400 | [13700] | 1.09 | 47 | 6.0 | −1.75 | 1.24 |
| NGC 7293 | 11000 | 9300 | 0.87 | 10 | 3.3 | −0.09 | 0.09 |
| NGC 7662 | 12800 | 10600 | 0.86 | 48 | 3.4 | −2.18 | 0.17 |
| IC   351 | 12000 | ... | ... | 45 | 3.9 | ... | 0.29 |
| IC   418 | 9700 | [ 8500] | 0.99 | 4.51 | 8.4 | −0.03 | 0.30 |
| IC  1747 | 10100 | ... | ... | 17 | 5.3 | ... | 0.33 |
| IC  2003 | 12100 | 14900 | 1.19 | 49 | 4.3 | −1.64 | 0.29 |
| IC  1297 | 10800 | [ 8300] | 0.77 | 36 | ... | −1.59 | 0.33 |

326

TABLE 2—*Continued*

| Nebula | $\overline{T}_e$ (K) [O III] | [N II] | $\overline{r}$ | I($\lambda4686$) or log $T_*$ | $10^4$ O/H | log [O II]/[O III] | c |
|---|---|---|---|---|---|---|---|
| (1) | (2) | (3) | (4) | (5) | (6) | (7) | (8) |
| IC 2149 | 10300 | 8700 | 0.87 | 4.56 | 2.0 | −0.88 | 0.25 |
| IC 2165 | 13900 | 9700 | 0.70 | 43 | 3.1 | −1.51 | 0.45 |
| IC 2448 | 13100 | ... | ... | 30 | 2.8 | ... | 0.10 |
| IC 2501 | 9800 | ( 9900) | 1.01 | 4.71/1 | 7.1 | −1.25 | 0.46 |
| IC 2553 | 10100 | 11700 | 1.16 | 22 | ... | −1.89 | 0.30 |
| IC 2621 | 13200 | [ 9900] | 0.75 | 42 | ... | −1.48 | 0.84 |
| IC 3568 | 10400 | ... | ... | 4.79/1 | 2.9 | ... | 0.19 |
| IC 4191 | 10500 | 12600 | 1.20 | 14 | ... | −1.46 | 0.66 |
| IC 4406 | 10500 | 9400 | 0.89 | 4.86/7 | 5.8 | −0.57 | 0.28 |
| IC 4593 | 8900 | 11400 | 1.28 | 4.63 | 3.3 | −1.12 | 0.05 |
| IC 4634 | 9800 | 11300 | 1.15 | 4.74 | 3.2 | −1.51 | 0.56 |
| IC 4776 | 8600 | [13900] | 1.62 | 4.76 | ... | −1.64 | 0.00 |
| IC 4846 | 10000 | 11700 | 1.17 | 4.79 | 4.4 | −1.65 | 0.47 |
| IC 5117 | 11600 | [12500] | 1.08 | 11 | 4.9 | −1.84 | 1.31 |
| IC 5217 | 11600 | (12000) | 1.02 | 10 | 3.4 | −1.80 | 0.34 |
| BB − 1 | 12900 | 10500 | 0.81 | 24 | 0.6 | −1.71 | 0.18 |
| BD + 30° | ... | 8600 | ... | 4.43 | 2.0 | 0.47 | 0.46 |
| Cn3-1 | 21500 | ( 7200) | 0.34 | 4.40 | 2.4 | 0.93 | 0.42 |
| DDM − 1 | 11800 | 11900 | 1.01 | 4.60 | ... | −0.70 | 0.08 |
| Ha1-55 | ... | 5300 | ... | 4.43 | ... | 0.63 | 1.11 |
| Ha4-1 | 12000 | ... | ... | 10 | 2.2 | ... | 0.12 |
| He2-5 | 11000: | 11500 | 1.05 | 4.66/2 | ... | −1.00 | 0.19 |
| He2-7 | 12700 | 12900 | 1.02 | 4.80/2 | ... | −1.16 | 0.26 |
| He2-108 | 9700 | ... | ... | 4.46 | 1.1 | ... | 0.45 |
| He2-131 | ... | [ 7100] | ... | 4.41 | ... | 1.08 | 0.19 |
| Hu1-1 | 12100 | 10200 | 0.84 | 16 | 4.2 | −0.56 | 0.43 |
| Hu1-2 | 17100 | 11600 | 0.68 | 101 | 2.0 | −1.20 | 0.59 |
| Hu2-1 | 9600 | 13300 | 1.38 | 4.56 | 3.7 | −0.77 | 0.49 |
| J 320 | 12600 | 13600 | 0.94 | 4.76/3 | 1.8 | −1.90 | 0.23 |
| J 900 | 12100 | 10600 | 0.88 | 42 | 3.5 | −1.32 | 0.71 |
| M1-1 | 15000 | 7300 | 0.51 | 96 | ... | −1.52 | 0.24 |
| M1-4 | 12800 | ... | ... | 5 | ... | ... | 1.94 |
| M1-5 | 9100 | 11700 | 1.29 | 4.58/3 | ... | −1.00 | 0.28 |
| M1-14 | 10500 | 9800 | 0.93 | 4.54 | 2.2 | −0.30 | 0.84 |
| M1-41 | ... | 10900 | ... | 71 | ... | ... | 3.82 |
| M1-67 | ... | 7400 | ... | <4.4 | 2.3 | >1.10 | 1.78 |
| M1-74 | 9300 | [10800] | 1.16 | 4.79 | 4.6 | −1.60 | 0.99 |
| M2-9 | ... | 9200 | ... | 4.47 | 5.2 | 0.23 | 1.32 |
| M2-50 | 12200 | ... | ... | 7 | 2.8 | ... | 0.66 |
| M3-1 | 11300 | 9900 | 0.81 | 4.70/1 | ... | −0.98 | 0.08 |
| M3-35 | 9000 | [11200] | 1.24 | 4.79/8 | ... | ... | 2.53 |
| M4-18 | ... | [ 6800] | ... | 4.34 | ... | ... | 1.00 |
| Me2-1 | 12400 | 11600 | 0.88 | 82 | ... | −1.71 | 0.11 |
| Me2-2 | 10800 | 13200 | 1.23 | 4.66 | 1.8 | −1.49 | 0.23 |
| PB-4 | 10800 | ... | ... | 21 | 2.7 | ... | 0.68 |
| PB-6 | 14400 | 11900 | 0.83 | 115 | ... | −0.22 | 0.54 |
| Ps-1 | 13100 | ... | ... | 4.43 | 0.7 | ... | 0.20 |
| Sn-1 | 10000 | ... | ... | 2 | 3.9 | ... | 0.22 |
| Vy1-2 | 9700 | 7700 | 0.80 | 25 | 7.9 | −1.65 | 0.05 |

[a] Both log $T_*$ and $I(\lambda4686)$ are given for $0 < I(\lambda4686) < 10$.
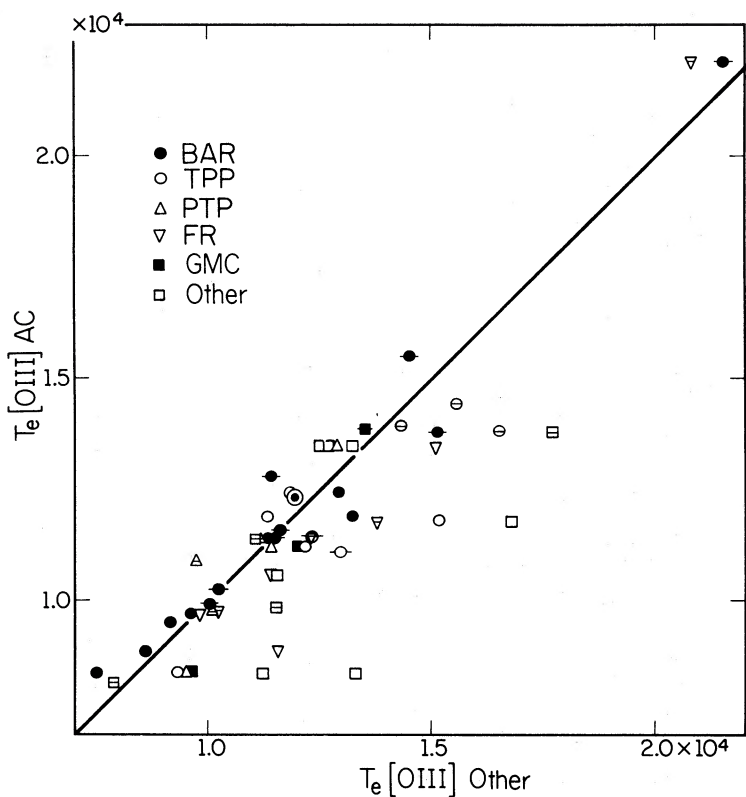
FIG. 1.—$T_e$[O III] from Aller and Czyzak (1979, 1983) vs. other values according to the caption. Those from Aller and Czyzak (1979) are denoted by a horizontal bar. The line is the 45° slope, as in Figs. 2–6.
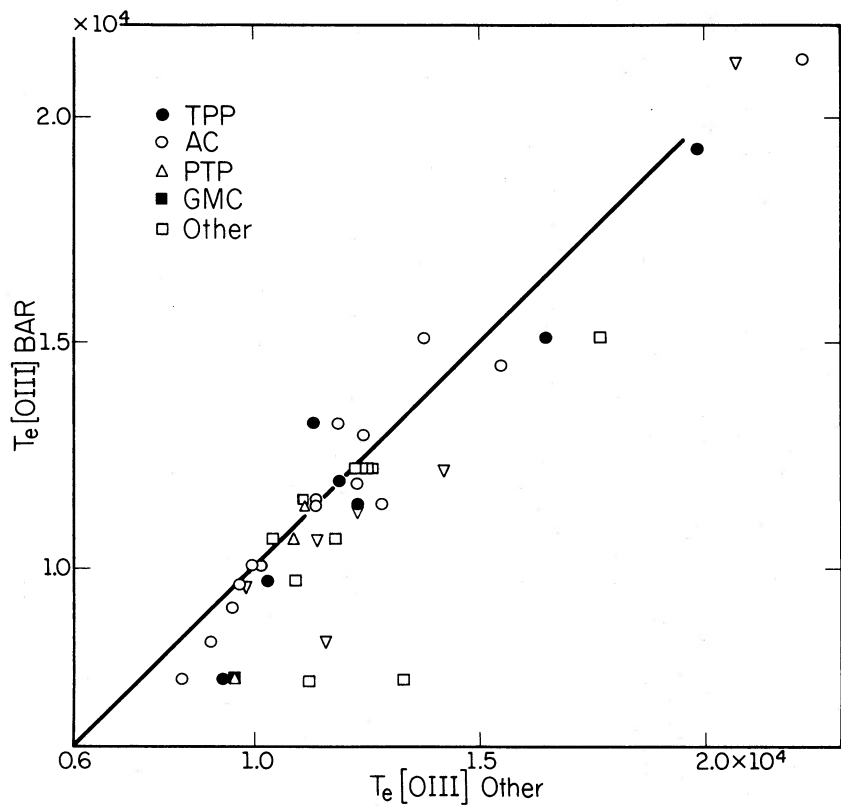


FIG. 2.—$T_e$[O III] from Barker (1978) vs. other values

328
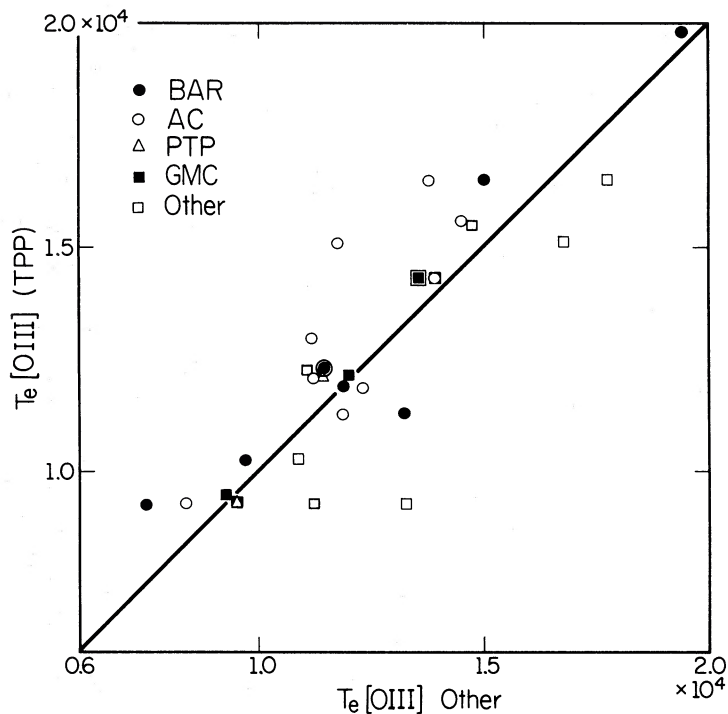
FIG. 3.—$T_e$[O III] from Torres-Peimbert and Peimbert (1977) vs. other values
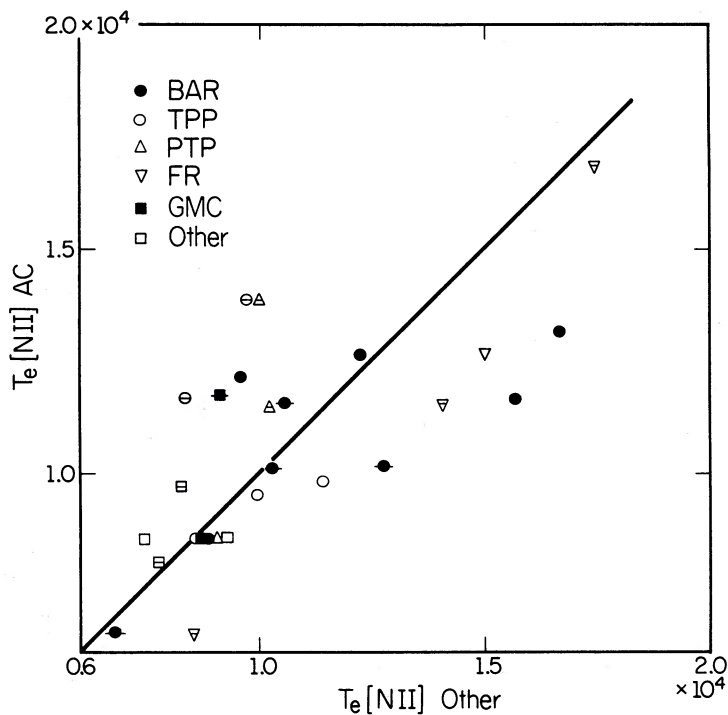


FIG. 4.—$T_e$[N II] from Aller and Czyzak (1979, 1983) vs. other values. Those from Aller and Czyzak (1979) are denoted by a horizontal bar.

329
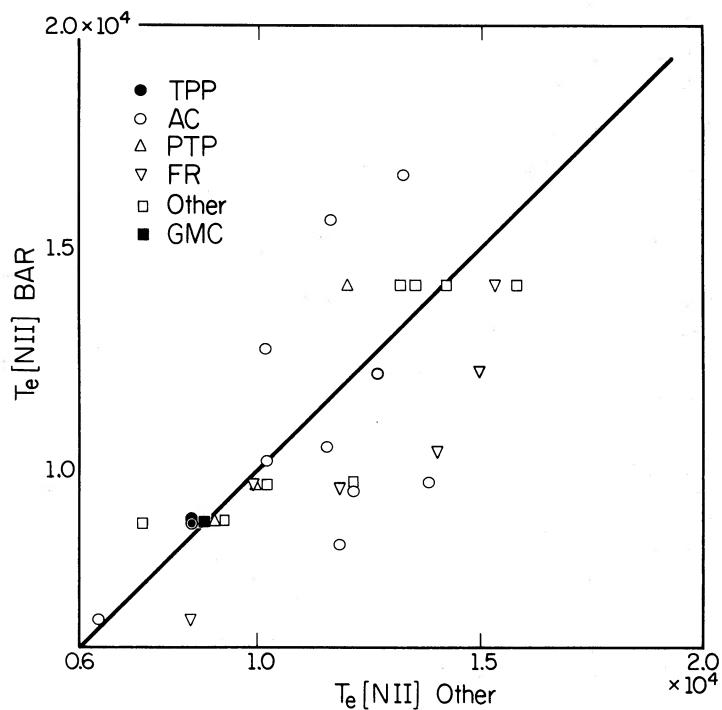
FIG. 5.—$T_e$[N II] from Barker (1978) vs. other values
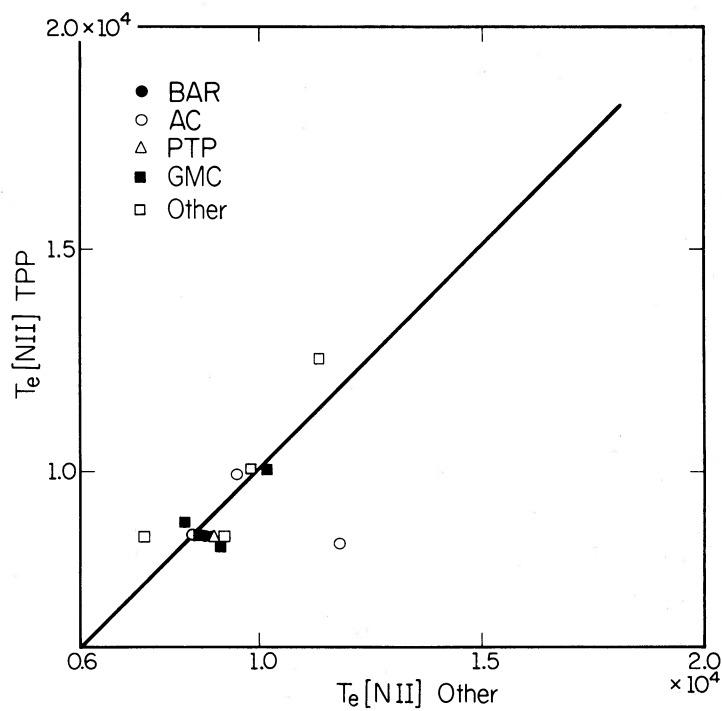


FIG. 6.—$T_e$[N II] from Torres-Peimbert and Peimbert (1977) vs. other values

parameterization of excitation, since log $T_*$ is directly related to the strength of [O III] (Kaler 1978a), and it is a slight modification of that used by Kaler (1978b), who used $He^{+2}/He$ instead of $I(\lambda 4686)$. The scheme produces good ionization curves for oxygen and neon, although there is a disconcerting discontinuity at the crossover point, which may be caused by artificially low scatter in the $T_*$ values related to the way in which they were derived. It is used here primarily because it is simple and is appropriate to easy use. The values of $I(\lambda 4686)$ or log $T_*$ are given in column (5) of Table 2. The former are derived from the references cited either in Table 1 or by Kaler (1976a) and from a compilation by Cahn and Kaler (1986). The log $T_*$ were derived from the Stoy method by Kaler (1976b, 1978a) and Goodrich and Dahari (1985); or from $I(\lambda 5007)$, as suggested by Kaler (1978a). For nebulae with $I(\lambda 4686) < 10$, both quantities are generally presented, from which it is seen that the joining of the two at log $T_* = 4.75$ is quite reasonable.

$T_e$[O III] is plotted against log $T_*-I(\lambda 4686)$ in Figure 7, where log $T_*$ is preferentially used where both are given. Triangles single out the four halo objects BB-1, DDM-1, Ha 4–1, and Ps 1, since these have extreme O/H ratios. M2–9 is excluded because of the disparity in the two regions observed. The steady rise in $T_e$ at the onset of He II is very noticeable. For nebulae with no He II in either spectra, no correlation is really discernable. The crosses show the medians of the distributions of points that fall between the dashed tick marks on the lower axis, excluding the halo objects and the anomalously high point representing Cn3–1; the vertical extents of the crosses show 90% confidence limits (Daniel 1978); the horizontal extents have no meaning. These crosses are connected by the curve, with small variations smoothed over where it seems appropriate. The dashed ticks, here and in Figures 9 and 12 below, are subjectively chosen so as to give the best sense of the temperature changes. It appears, then, that $T_e$[O III] averages near the canonical 10,000 K (actually 10,200 K) for low-

excitation nebulae, and that for $I(\lambda 4686) > 0$, $T_e = [9700 + 58I(\lambda 4686)]$ K. There is some slim suggestion that $T_e$[O III] may drop below 10,000 K near log $T_* \approx 4.65$ and then climb again as $T_*$ decreases, but this possibility may be only an artifact of the small number of nebulae available for this region of the diagram. This upward trend is buttressed by the strange object Cn3–1, for which $T_e$[O III] is over 20,000 K, as found by three independent studies. This high value may yet not be real, however, and may be a result of an unaccounted-for high density near the nebular center. We return to the subject below when we compare [N II] and [O III] temperatures.

The wide scatter present in Figure 7 for a given excitation is real and is due to variations in the O/H ratio. Oxygen is the primary coolant of a nebula, and as O/H goes down, $T_e$ must go up. Kaler's (1980) O/H ratios are given in column (6) of Table 2. $T_e$[O III] is plotted against them for five excitation groups in Figure 8, where we see again the positive correlation between $I(\lambda 4686)$ and $T_e$ and also the negative correlation between $T_e$ and O/H. Within the scatter, the slopes for each excitation group are parallel to one another, at roughly $-600$ K per $10^{-4}$ O/H unit. Note that the atomic parameters used for the calculation of O/H are somewhat different from those employed here in the determination of $T_e$, so that the variables in Figure 8 are not entirely consistent. Recomputation of O/H is beyond the scope and purpose of this paper, and in any case is probably unnecessary since any adjustments would likely be lost within the other uncertainties.

Since O/H has a strong and continuous dependence on population type, the scatter in Figure 7 then is seen to be a result of a mixture of stellar populations within the set of observed planetaries. If we try to estimate $T_e$[O III] on the basis of log $T_*-I(\lambda 4686)$, the value will be appropriate to an intermediate stellar type. From Figure 8 and from Kaler's (1980) correlation between mean O/H and population type, we might respectively augment or reduce the mean $T_e$[O III] by roughly
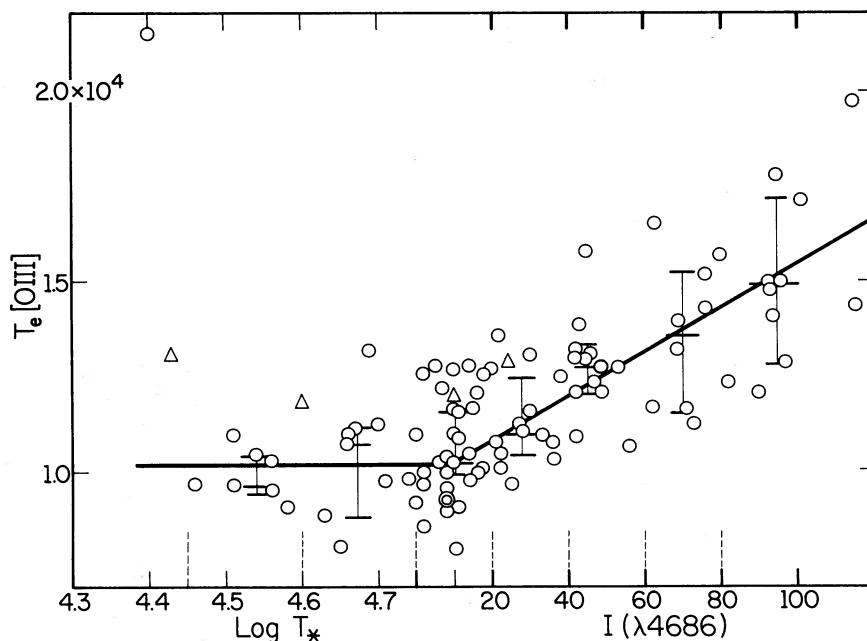


FIG. 7.—Mean $T_e$[O III] vs. the combination of log $T_*$ and $I(\lambda 4686)$. *Triangles*, the halo nebulae. *Large crosses*, medians of the point distributions within the dashed tick marks on the lower axis, from which the triangles are excluded. Points on a tick are counted to the high side of it. 90% confidence limits are represented by the vertical extents of the bars. The solid line is passed through the medians.
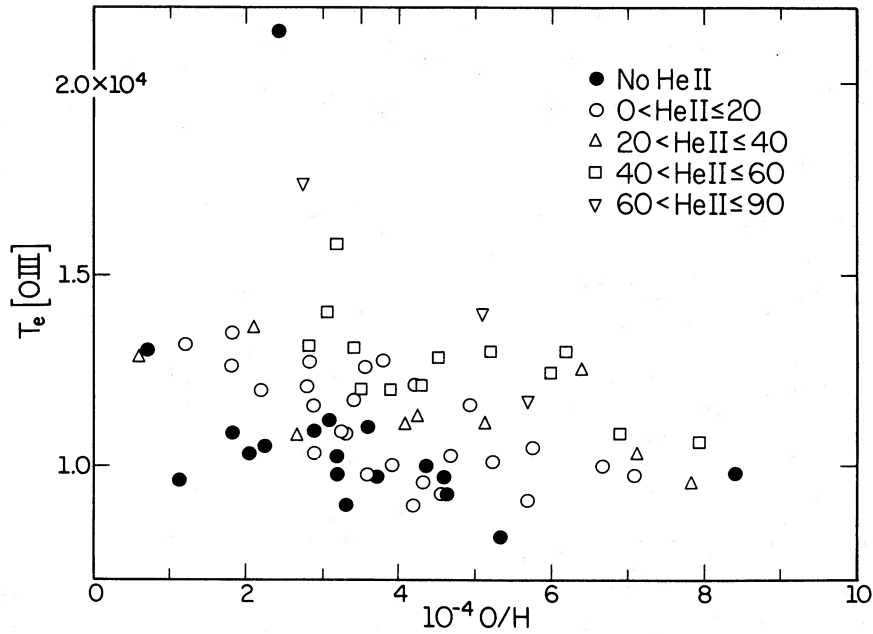
FIG. 8.—$T_e$[O III] vs. O/H for six excitation groups defined by the strength of He II $\lambda4686$ as indicated in the caption

1000 K for nebulae clearly known to be Population II ($|v_r(\mathrm{LSR})| > 85$ km s$^{-1}$) or Population I. A criterion for the latter might be significant enrichment of helium, since the He/H ratio is not itself very sensitive to $T_e$. However, to some degree this population correlation is already built into that between $T_e$ and excitation, since excitation is correlated with O/H (see Fig. 8 and Kaler 1980). Thus any such corrections should be applied with caution. One must also be careful not to introduce circular reasoning into an analysis that employs these correlations.

The correlation between $T_e$[N II] and log $T_*$–$I(\lambda4686)$ is displayed in Figure 9. N$^+$ is much more sensitive to collisional deexcitation than O$^{+2}$, and the temperatures are uncertain for higher densities. Consequently, nebulae with density parameters of $x = 1$ and $x > 1$ are so noted in the figure. Again, the curve connects (with some smoothing) the crosses that show the medians of the distributions between the dashed ticks on the lower axis, with 90% confidence limits as indicated above; the halo nebulae and the one bulge object (Ha 1–55) are excluded from the counts because of anomalous abundances.
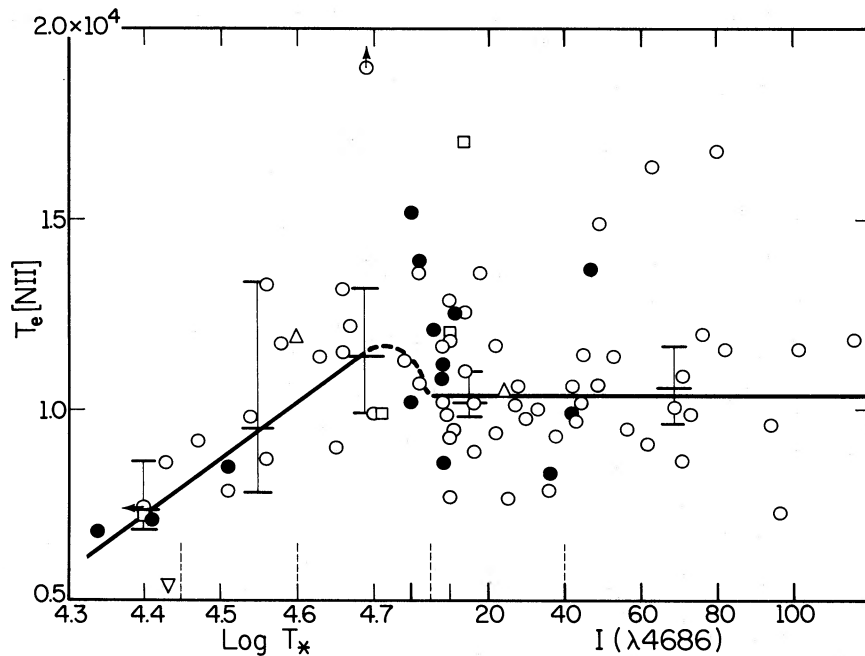


FIG. 9.—Mean $T_e$[N II] vs. the combination of log $T_*$ and $I(\lambda4686)$. *Triangles*, halo nebulae; *open circles*, $x_N < 1$; *squares*, $x_N = 1$; *filled circles*, $x_N > 1$; *downward triangle*: bulge nebula. The crosses again represent the medians of the points falling between the dashed ticks on the lower axis; the solid curve connects them. Halo and bulge nebulae are excluded from the medians, as are nebulae with $x_N > 1$, except for log $T_* < 4.45$, for which all points (except the bulge object) are accepted.

The objects with $x > 1$ are also excluded because of uncertainty in the values of the temperatures, except for log $T_*$ < 4.45, for which they are needed to define the curve. Here, we see something very different. The behavior of $T_e$[N II] is almost the reverse of that of $T_e$[O III]. Now for $I(\lambda 4686) \gtrsim 5$, the median temperature stays roughly constant near the canonical 10,000 K (actually 10,300 K). Then, as we proceed to excitations lower than $I(\lambda 4686) \approx 5$, $T_e$ appears first to rise to nearly 12,000 K and then quite clearly drops to ~7000 K at the lowest stellar temperatures, according to the rule $T_e$[N II] = (14,670 log $T_*$ − 57,330) K for log $T_*$ < 4.775. The sudden rise near the crossover in the abscissa variable may well be related to the discontinuity discussed above for the ionization curves. Note, however, that the error bars are large and that we cannot exclude a flat temperature distribution near 10,000 K down to log $T_*$ as low as 4.55 or so. There does seem to be a certain plunge at the lowest central star temperatures, but more data are needed to confirm the rise near log $T_* = 4.7$.

Assuming that the above rise is actually present, some further analysis suggests that the higher [N II] temperatures occur for lower optical depths where the N$^+$ shell is quite thin. The size of the O$^+$ shell to that containing the O$^{+2}$ provides a good indicator of optical depth, and for subsequent analysis log $\{I([O II] \lambda 3727)/I([O III] \lambda 5007, \lambda 4959)\}$ = log [O II]/[O III] is given in column (7) of Table 2. The quantity $T_e$[N II] is plotted against this parameter in Figure 10, where we clearly see that, with some exceptions, the temperature rises as the O$^+$ (and concomitantly the N$^+$) shell shrinks in size at the nebula's periphery. From Table 2, 70% of the higher temperature nebulae ($T_e$[N II] $\geq$ 11,000 K) that have log [O II]/[O III] $\leq$ 1.4 also are within the intermediate range of stellar temperature, with $I(\lambda 4686) \leq 20$ and log $T_* > 4.55$ (whether or not we include or exclude nebulae with $x > 1$), thus complementing the distribution seen in Figure 9.

The scatter in Figures 9 and 10 is again caused by variations in oxygen abundance. Figure 11 shows $T_e$[N II] plotted against O/H, where we see a negative correlation similar to that found for $T_e$[O III] in Figure 8. Since $T_e$[N II] is not very dependent on $I(\lambda 4686)$, Figure 11 shows the nebulae divided by excitation as expressed by log [O II]/[O III]. Unlike Figure 8, in which the slopes are roughly the same for all excitation classes, the [N II] temperature gradient against O/H seems to steepen noticeably as we proceed to lower [O II]/[O III] intensity ratios. For estimation of $T_e$[N II] from log $T_*$–$I(\lambda 4686)$, it again seems reasonable to add ~1000 K to the mean for Population II nebulae and to subtract it for Population I; finer corrections could be made from Figure 11 if log [O II]/[O III] is known.

Finally, in Figure 12, we look at the relation between the [N II] and [O III] temperatures. Here $\bar{r}$, the mean of the ratios of $T_e$[N II]/$T_e$[O III] as found from individual reference sources, is displayed. We see that as excitation increases, the points define a locus that starts below unity, rises above it, then falls. The crosses against indicate the medians within the dashed tick marks on the lower axis, with 90% confidence limits as before. Here, we include the halo and bulge nebulae, and also include Cn3–1 as a single defining point at low $T_*$ in order to establish a limiting case. Again, we see a sudden change in the distribution near the onset of He II $\lambda 4686$, reminiscent of a discontinuity. The smoothed solid curve passed through the medians shows a rise with increasing excitation caused by the flat $T_e$[O III] and rising $T_e$[N II] distributions below log $T_* \approx 4.7$, followed by a fall caused by the flattening of $T_e$[N II] and the rise in $T_e$[O III] at the onset of He$^{+2}$. However, note again that the confidence limits will allow a flat distribution for nebulae without $\lambda 4686$, with $\bar{r}$ between 1.0 and 1.25.

The dashed line shows $\bar{r}$ as a function of log $T_*/I(\lambda 4686)$ found from the separate distributions of $T_e$[N II] and $T_e$[O III]
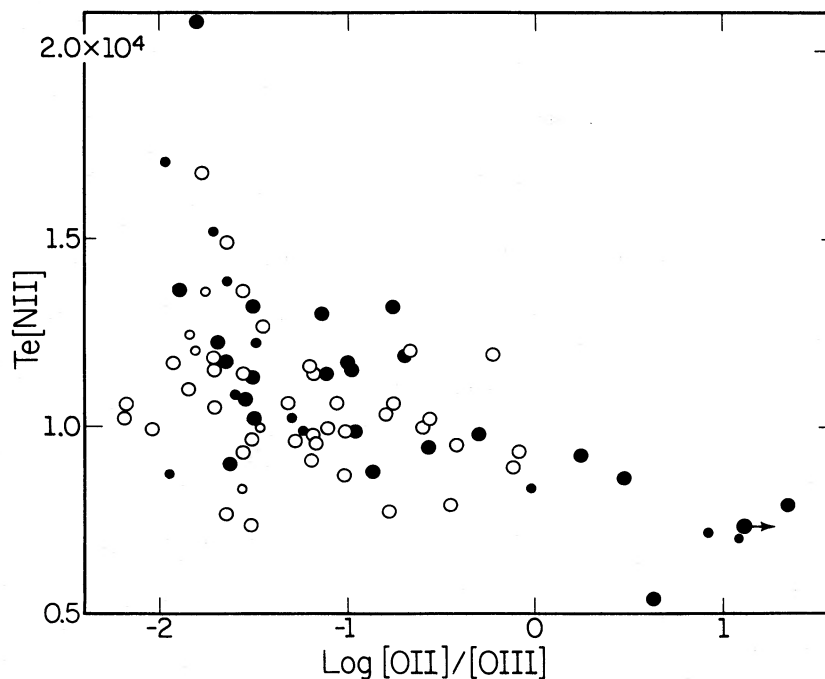


FIG. 10.—$T_e$[N II] vs. log $I([O II] \lambda 3727)/I([O III] \lambda 4959, \lambda 5007)$ = log [O II]/[O III]. *Small symbols*, nebulae with $x \geq 1$; *filled symbols*, nebulae with $T_*$ listed in Table 2, for which $I(\lambda 4686) < 10$.
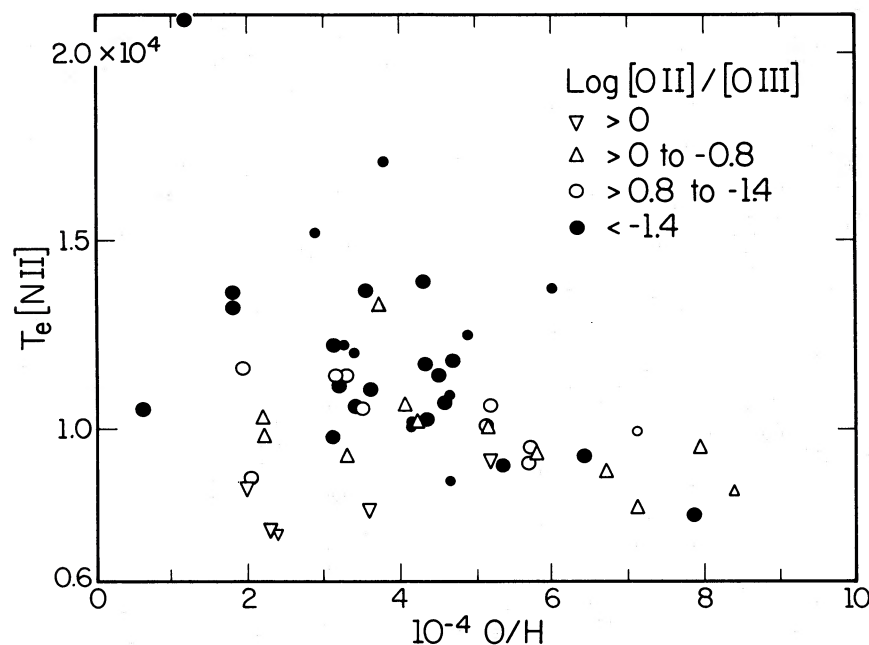
FIG. 11.—$T_e$[N II] vs. O/H for various excitation groups as defined by log [O II]/[O III]. Small symbols denote $x \geq 1$.

by dividing the curve of Figure 9 by that of Figure 7. This curve does *not* use Cn3–1 as a defining point and is probably superior, since it includes additional data: nebulae for which one temperature has been determined but not the other. Except at the lowest excitation (low $T_*$), the two curves agree quite well. The additional data from nebulae with only $T_e$[N II] values support the rise in the curve as log $T_*$ increases and is counter to the possibility of the flat distribution mentioned above.

We see here that Torres-Peimbert and Peimbert's (1977) assessment of $T_e$[O III]/$T_e$[N II] = 1.25 for nebulae with $I(\lambda4686) > 25$ is quite good. The surprise, however (if one adopts the curves of Fig. 12), is that the two temperatures do not, except at two points, come into equality, as in the past has always been assumed. It seems quite likely that the [N II] temperature can exceed that found from [O III]; at lower $T_*$ it appears again to be notably depressed. Firm confirmation must await additional data.

### IV. TEMPERATURE GRADIENTS

Planetary nebulae display a clear stratification of ions in which the lower stages of ionization are farther from the central star than the higher. This feature is shown both observationally, via monochromatic photographs (e.g., Aller 1956), and theoretically, via models (e.g., Osterbrock 1974). The ratio of [N II] and [O III] temperatures then indicates the sign of the outwardly directed temperature gradient. In this section, let us assume that the curves of Figures 7, 9, and 12 are correct as they stand and that they represent some sort of mean averaged over the widely diverse conditions actually found among planetaries. We see from Figure 12 that for both high and low excitation, the temperature gradient is negative with increasing distance from the central star (i.e., temperature falls from the center of the $O^{+2}$ radiating region to the middle of the $N^+$ or $O^+$ zone) but reverses just to the low-excitation side of the onset of $He^{+2}$. The average position of the positive gradient

coincides quite well with maximum nebular $O^{+2}$ ionization, as seen from Kaler's (1978a) Figure 1.

At low excitation (or low $T_*$), $N^+$ (and $O^+$) dominates, and whatever $O^{+2}$ exists is contiguous to the central star. $T_e$[N II] depends on the energy input from the star, and as $T_*$ drops, so does this electron temperature. But as $T_*$ decreases, so does the size of the $O^{+2}$ zone, whose center of distribution moves closer to the star, apparently offsetting the decreased energy available for ionization. Possibly $T_e$[O III] may even go up, culminating in an object like Cn3–1 in which the [O III] temperature is much higher than $T_e$[N II], because $O^{+2}$ is so close to the energy source. Alternatively, as mentioned earlier, an increase in density may be present this close to the nucleus, artificially raising our determination of temperature.

Now, as $T_*$ rises from a low level, the $O^{+2}$ zone grows until at about log $T_* = 4.56$, the amounts of $O^{+2}$ and $O^+$ are about equal (see Kaler 1978a). From Figure 12, we see that it is just at this point that $T_e$[N II] = $T_e$[O III]. At log $T_* = 4.7$, $O^{+2}$ very nearly fills the entire nebula. Whatever $O^+$ and $N^+$ there is must now exist in a thin shell around the nebula's periphery. It is in this state that the gradient is positive, or at least becomes flat.

As helium becomes doubly ionized, the center of the nebula begins to become filled with $O^{+3}$, and the $O^{+2}$ zone moves outward, taking on the form of a shell. The increasing ultraviolet luminosity that causes a rise in the ionization level also produces an increase in the [O III] temperature. This behavior is analogous to the increase in $T_e$[N II] with $T_*$ that takes place at low temperatures when $O^+$ and $N^+$ are dominant. As both the $O^{+2}$ and $N^+$ shells move otward from the star, the gradient reverses again and continues to steepen as the nebula fills with $He^{+2}$ and the higher ionization states of oxygen.

This qualitative description must now be tested against quantitative modeling procedures. The empirical relation between the [N II] and [O III] temperatures in fact provides an interesting test for the validity of nebular models.
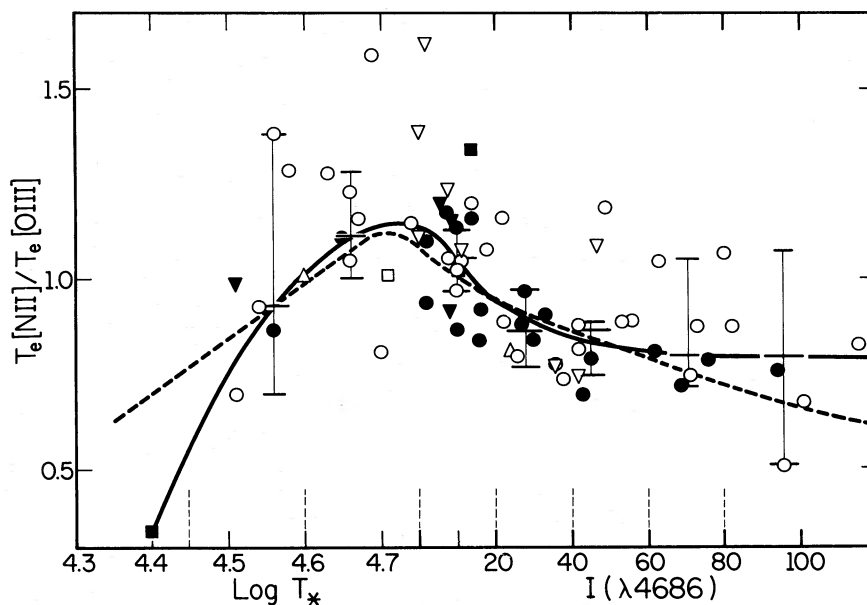
Fig. 12.—Mean $T_e[\text{N II}]/T_e[\text{O III}] = \bar{r}$ vs. the combination of $\log T_*$ and $I(\lambda4686)$. *Filled symbols*, nebulae with two or more observations; *boxes*, $x = 1$; *downward triangles*, $x > 1$; *upward triangles*, halo nebulae. The crosses again represent the median of the points falling between the dashed ticks on the lower axis, excluding the downward triangles. *Solid curve*, the best-fit distribution derived from the medians for this figure, including Cn3–1 as a lower defining point; *dashed curve*, the relation found by dividing the distribution of Fig. 9 for $T_e[\text{N II}]$ by that for Fig. 7 for $T_e[\text{O III}]$.

## V. APPLICATIONS AND SUMMARY

In an ideal world, we would have line intensities available for all diagnostic ions. However, in practice, critical lines are frequently unavailable for a variety of reasons. We see from Table 2 that 23% of the nebulae in this study have no [N II] temperatures available, and eight have $T_e[\text{N II}]$ but no $T_e[\text{O III}]$. Extremes in excitation can cause some lines to be unobservably weak, as discussed in § I. In addition, the low surface brightnesses of large nebulae can make the auroral lines so weak that no temperatures can be derived at all; high interstellar reddening can make the blue spectral region impossible to observe, so that only $T_e[\text{N II}]$ is available; and we are frequently saddled with limited detector coverage and weather problems.

As we probe toward dimmer planetaries, we will increasingly encounter a problem with incomplete data sets, and we will need methods to enable us to extract pertinent physical information from only a few accessible lines. Kaler (1985) began to attack this problem by developing a method for the estimation of N/O ratios from red spectra wherein the [O II] lines are not observed, by using correlations between the intensities of [O II] $\lambda3727$ and [O I] $\lambda6300$ or [S II] $\lambda6723$. With the correlations established between excitation and $T_e[\text{O III}]$, $T_e[\text{N II}]$, and $\bar{r} = T_e[\text{N II}]/T_e[\text{O III}]$ in Figures 7, 9, and 12, we are now able to estimate with some accuracy the electron temperatures of nebulae from $I(\lambda4686)$, or, for lower excitation objects, from $T_*$, and from $I(\lambda5007)$ through the correlation established by Kaler (1978a).

The user of this work may employ the curves of Figures 7 and 9 directly or the simplifications given above. To summarize:

for $I(\lambda4686) = 0$, $T_e[\text{O III}] = 10,200$ K ,

$\qquad\qquad T_e[\text{N II}] = (14,670 \log T_* - 57,330)$ K ;

for $I(\lambda4686) > 0$, $T_e[\text{O III}] = [9700 + 58\, I(\lambda4686)]$ K ,

$\qquad\qquad T_e[\text{N II}] = 10,300$ K .

If there is a clear indication of population type, it is recommended that 1000 K be added for Population II and subtracted for Population I. Figure 12 should be used to find either temperature when the other is known. The user should be well aware that these are median relations, and, as can be seen from the figures, values for any given nebula can be considerably different. Even the medians are insecure for lower excitation when there is a dearth of data. However, even given the above limitations, we have here a significant advance in the subject.

Since electron temperature is a function of both excitation and O/H, it is in fact possible to get a rough estimate of O/H if $T_e$ and either $I(\lambda4686)$ or $\log T_*$ is known. We can, for example, determine the excitation group defined in Figure 8, then read off the O/H that corresponds to $T_e$. Admittedly, the procedure is crude, but it could be useful if [O II] and the He I lines are not observable. The latter are used with He II to estimate the abundance of the higher oxygen ionization stages, $O^{+3}$ and $O^{+4}$.

It is most important that the curve of Figure 12 be used in the calculations of N/O ratios when these are determined through the optical $N^+$ and $O^+$ lines. It is simply not satisfactory to equate $T_e[\text{N II}]$ to $T_e[\text{O III}]$ when, say, only the latter is known. For example, a variation in $\bar{r}$ from 0.75 to 1.15 between $\log T_* = 4.4$ and 4.7 can cause a relative error in N/O of a factor of 2. Kaler (1979) found that $N^+/O^+$ was negatively correlated with $T_*$ for $\log T_* < 4.65$. At least part (though possibly not all) of the correlation was produced by assuming equality of the [N II] and [O III] temperatures. Since $T_e[\text{O III}]$ is available and is $\sim 10,000$ K, $T_e[\text{N II}]$ is overestimated, resulting in a systematic increase in N/O as $T_*$ falls. A similar effect can be seen in the increase in the [S II] to [O II] intensity ratios for decreasing $T_*$, as illustrated in Kaler's (1981) Figure 4. The strengths of the [O II] lines are considerably more sensitive to $T_e$ than are those of [S II]. About half the observed slope can be accounted for by the decrease in $T_e[\text{N II}]$ illustrated herein. We do not know the conditions in the $S^+$ zone, which

may well not be coincident with $N^+$, and for which electron temperature variations may be more extreme.

The analysis described in this paper defines $T_e$ for intermediate and higher excitation nebulae quite well. However, there is a clear paucity of observations at low excitation: these objects are relatively rare. A larger number of nebulae with low-temperature nuclei should be observed with high signal-to-noise ratios so as to derive $T_e[O \text{ III}]$, in order better to establish $\bar{r}(\log T_*)$, to see whether or not the extraordinary temperature dichotomy for Cn3–1 is real and can be found in other objects, and to see whether or not a real reversal in the temperature gradient is present.

## REFERENCES

Aller, L. H. 1956, *Gaseous Nebulae* (New York: Wiley).
———. 1984, *Physics of Thermal Gaseous Nebulae* (Dordrecht: Reidel).
Aller, L. H., and Czyzak, S. J. 1978, *Proc. Nat. Acad. Sci.*, **75**, 1.
———. 1979, *Ap. Space Sci.*, **62**, 397.
———. 1983, *Ap. J. Suppl.*, **51**, 211.
Aller, L. H., and Epps, H. W. 1976, *Ap. J.*, **204**, 445.
Aller, L. H., Keyes, C. D., and Czyzak, S. J. 1981a, *Ap. J.*, **250**, 596.
Aller, L. H., Keys, C. D., Ross, J. E., and O'Mara, B. J. 1981b, *M.N.R.A.S.*, **197**, 647.
Barker, T. 1978, *Ap. J.*, **219**, 914.
———. 1979, *Ap. J.*, **227**, 863.
———. 1980, *Ap. J.*, **240**, 99.
———. 1983, *Ap. J.*, **267**, 630.
———. 1984, *Ap. J.*, **284**, 589.
———. 1985, *Ap. J.*, **294**, 193.
———. 1986, *Ap. J.*, **308**, 314.
Barker, T., and Cudworth, K. M. 1984, *Ap. J.*, **278**, 610.
Brocklehurst, M. 1971, *M.N.R.A.S.*, **153**, 471.
Cahn, J. H., and Kaler, J. B. 1986, in preparation.
Czyzak, S. J., and Aller, L. H. 1979, *M.N.R.A.S.*, **188**, 229.
Clegg, R. E. S., Seaton, M. J., Peimbert, M., and Torres-Peimbert, S. 1983, *M.N.R.A.S.*, **205**, 417.
Daniel, W. W. 1978, *Applied Nonparametric Statistics* (Boston: Houghton-Mifflin), p. 37.
Danziger, I. J., Frogel, J. A., and Persson, S. E. 1973, *Ap. J. (Letters)*, **184**, L29.
Dopita, M. A. 1977, *Ap. Space Sci.*, **48**, 437.
Dufour, R. J. 1984, *Ap. J.*, **287**, 341.
Feibelman, W. A., Aller, L. H., Keyes, C. D., and Czyzak, S. J. 1985, *Proc. Nat. Acad. Sci.*, **82**, 2202.
French, H. B. 1981, *Ap. J.*, **246**, 434.
Goodrich, R. W., and Dahari, O. 1985, *Ap. J.*, **289**, 342.
Gutiérrez-Moreno, A., Moreno, H., and Cortés, G. 1985, *Pub. A.S.P.*, **97**, 397.
Hawley, S. A. 1978, *Pub. A.S.P.*, **90**, 370.
Hawley, S. A., and Miller, J. S. 1977, *Ap. J.*, **212**, 94.
Hawley, S. A., and Miller, J. S. 1978a, *Ap. J.*, **220**, 609.
———. 1978b, *Pub. A.S.P.*, **90**, 39.
Kaler, J. B. 1970, *Ap. J.*, **160**, 887.
———. 1976a, *Ap. J. Suppl.*, **31**, 517.
———. 1976b, *Ap. J.*, **210**, 843.
———. 1978a, *Ap. J.*, **220**, 887.
———. 1978b, *Ap. J.*, **225**, 527.
———. 1979, *Ap. J.*, **228**, 163.
———. 1980, *Ap. J.*, **239**, 78.
———. 1981, *Ap. J.*, **244**, 54.
———. 1983, *Ap. J.*, **271**, 188.
———. 1985, *Ap. J.*, **290**, 531.
Kaler, J. B., Aller, L. H., Czyzak, S. J., and Epps, H. W. 1976, *Ap. J. Suppl.*, **31**, 163.
Mendoza, C. 1983, in *IAU Symposium 103, Planetary Nebulae*, ed. D. Flower (Dordrecht: Reidel), p. 245.
Miller, J. S., and Mathews, W. G. 1972, *Ap. J.*, **172**, 593.
O'Dell, C. R. 1963, *Ap. J.*, **138**, 1018.
———. 1964, private communication.
Osterbrock, D. E. 1974, *Astrophysics of Gaseous Nebulae* (San Francisco: Freeman).
Peimbert, M. 1973, *Mem. Soc. Roy. Sci. Liège*, Series 6, Vol. **5**, p. 79.
Peimbert, M., and Torres-Peimbert, S. 1971, *Bol. Obs. Tonantzintla y Tacubaya*, **5**, 3.
Price, C. M. 1981, *Ap. J.*, **247**, 540.
Seaton, M. J. 1960, *Rept. Progr. Phys.*, **23**, 313.
Shields, G. A., Aller, L. H., Keyes, C. D., and Czyzak, S. J. 1981, *Ap. J.*, **248**, 569.
Torres-Peimbert, S., and Peimbert, M. 1977, *Rev. Mexicana Astr. Ap.*, **2**, 181.
———. 1979, *Rev. Mexicana Astr. Ap.*, **4**, 341.
Torres-Peimbert, S., Rayo, J. F., and Peimbert, M. 1981, *Rev. Mexicana Astr. Ap.*, **6**, 315.
Whitford, A. E. 1958, *A.J.*, **63**, 201.

JAMES B. KALER: Department of Astronomy, University of Illinois, 349 Astronomy Building, 1011 West Springfield Avenue, Urbana, IL 61801